Work published on IEEE Trans. on Instrumentation and Measurement, , 64(5), pp. 1129-1139, 2015,
DOI 10.1109/TIM.2014.2363752

On the Accuracy of Phasor Angle Measurements in Power Networks

Grazia Barchi[1], *Graduate Student Member, IEEE,* Daniele Fontanelli[2], *Member IEEE,*
David Macii[2], *Senior Member, IEEE,* Dario Petri[2], *Fellow, IEEE*

[1]Dep. of Information Engineering and Computer Science, University of Trento
[2]Dep. of Industrial Engineering, University of Trento
E-mail: {grazia.barchi,daniele.fontanelli,david.macii,dario.petri}@unitn.it

***Abstract* — As known, Phasor Measurement Units (PMUs) greatly enhance smart grid monitoring capabilities with advantageous impacts on power network management. Generally, PMUs accuracy is expressed in terms of Total Vector Error (TVE), which comprises the joint effect of both angle and magnitude errors, thus possibly concealing the algorithm ability to measure phase. Some recent research works emphasize the importance of measuring current or voltage phasor angle with high accuracy (in the order of a few mrad) at the distribution level. Since this issue is seldom considered in the literature, in this paper the phase measurement accuracy of three algorithms, namely the basic DFT, the windowed Taylor-Fourier Filter (WTFF) and the Interpolated Dynamic DFT (IpD^{2}FT) estimator, is extensively analyzed by means of simulations performed in various conditions described in the Standards IEEE C37.118.1:2011 and EN 50160:2010. In addition, some meaningful considerations about the uncertainty contributions due to imperfect synchronization are reported.**

Keywords* — *Power systems, estimation, Discrete Fourier Transform (DFT), uncertainty.

I. INTRODUCTION

The implementation of smart grids requires increasingly sophisticated and flexible instruments for fine-grained monitoring and control, both in steady-state and transient conditions (e.g. for voltage dip detection [1]). Till now, network state estimation and detection of anomalous events have generally relied on measurements of bus voltage magnitude, active/reactive power injections and active/reactive power flows in stationary or quasi-stationary conditions [2]. However, in the near future, significant voltage or current waveform changes will have to be tracked in real-time. This task is expected to be accomplished by specific instruments such as the so-called *Phasor Measurement Units* (PMUs), i.e. instruments able to measure voltage and current phasors, the waveforms frequency and their rate of change of frequency (ROCOF), synchronized to the Coordinated Universal Time (UTC) [3]. Originally conceived for *Wide Area Monitoring Systems* (WAMS) at the transmission level, PMUs have become particularly interesting at the distribution level [4],[5], e.g. for protection and stability assessment [6], distribution system state estimation [7], fault detection/location [8], power quality evaluation [9] and management of fast time-varying loads [10]. Various algorithms for phasor estimation exist [11],[12]. Quite importantly, the features of PMUs for next-generation distribution systems are generally different from those at the transmission level [13]. Indeed, the phase offsets of waveforms in different points of the network are normally quite small, but, at the same time, they may vary considerably (both in terms of amplitude and speed), as a result of significant changes in generation or load profiles. In fact, not only the voltage magnitudes, but also the phasor angles depend on the levels of demand and distributed generation (e.g. based on wind farms) at a given time [14]. For this reason, the PMUs for distribution systems are expected to exhibit stricter accuracy requirements than those reported in the IEEE Standards C37.118.1:2011 and C37.118.1a:2014 for transmission networks [15],[16]. Such requirements are described in [17]. In particular, a PMU for distribution systems should not only track waveform phasors, frequency and ROCOF in real-time under dynamic conditions [18],[19], but it should be also able to measure phasor angles with uncertainty in the order a few mrad or less [1],[5], as it is confirmed by the specifications of some novel instruments currently under development [20].

When different PMUs, or, simply, different phasor estimation algorithms are compared, the performance parameter that most frequently is used to express accuracy is the so-called *Total Vector Error* (TVE). This parameter includes, but also partially conceals, the effect of phase errors. As a consequence, the accuracy of phase measurements alone are seldom analyzed in the literature. Generally, phase errors result from three main contributions, i.e. unwanted phase shifts introduced by instrument transformers (which are in the order of a few crad) [21], offsets caused by the estimation algorithm itself and deviations due to the limited time synchronization accuracy [9],[22] or, sometimes, to the need to reconstruct the phasor values at times different from the reported ones [23]. The contribution of instrument transformers is not related to the PMU, so it is out the scope of this paper. The uncertainty contributions due to the synchrophasor estimation algorithm is probably the most interesting, as it depends also on the features of the signals to be monitored. This paper extends the preliminary results reported in [24] by comparing the results provided by three techniques, i.e. the typical windowed Discrete Fourier Transform (DFT) synchrophasor estimator [25], the Interpolated Dynamic DFT (IpD^{2}FT) algorithm [26], and the Taylor-Fourier Filter (TFF), firstly introduced in [19] and further improved through windowing in [27].

It is worth emphasizing that the proposed comparison is not exhaustive. In fact, just general conclusions can be drawn from the presented analysis. Several variants of the considered algorithms exist to address possible drawbacks arising in different operating conditions.

In the rest of this paper, after introducing the general phasor model in Section II, the DFT-based phasor estimator is shortly recalled in Section III. The IpD^{2}FT and windowed TFF (WFFT) estimators instead, which are based on a dynamic phasor model, are described in Section IV. A comparison about the computational complexity of the various algorithms is shortly reported in Section V. In all cases, the worst-case phasor angle measurement uncertainty is evaluated through extensive simulations in Section VI under the assumption that the input waveforms meet the requirements of Standards IEEE C37.118.1:2011 or EN 50160:2010. In fact, the latter document is specifically focused on power quality requirements at the distribution level and it "specifies the main characteristics of the voltage at a network user's supply terminals in low, medium and high voltage AC electricity networks under normal operative conditions" [28]. Finally, in Section VII, the additional contributions due to sampling jitter, time synchronization uncertainty and imperfect phasor reconstruction at different times (which are common issues for all considered estimators) are analyzed and quantified.

II. Phasor Model Definition

Let $x(t)$ be a general electrical waveform of frequency $f_x = f_0(1+\zeta)$, where f_0 is the nominal value (i.e. 50 or 60 Hz) and ζ is a static fractional frequency deviation. If the PMU nominal sampling rate is $f_s=M\cdot f_0$ (with M integer) the discrete-time sequence in an observation interval centered at the UTC reference time t_r (with $r \in Z$) can be expressed as [19]

$$\begin{aligned} x_r[n] &= \mathbf{Re}\left\{A\left[1+\varepsilon_a(t_r+nT_s)\right]\cdot e^{j\left[2\pi f_x(t_r+nT_s)+\varepsilon_p(t_r+nT_s)+\phi\right]}\right\} = \\ &= \mathbf{Re}\left\{\sqrt{2}\,p_r[n]\,e^{j\frac{2\pi}{M}(1+\zeta)n}\right\} = \mathbf{Re}\left\{\sqrt{2}\,p_r'[n]\,e^{j\frac{2\pi}{M}n}\right\} \end{aligned} \quad (1)$$

where the operator $\mathbf{Re}\{\cdot\}$ extracts the real part of its argument, A is the waveform amplitude, $T_s=1/f_s$ is the nominal sampling period, ϕ is the waveform initial phase and $\varepsilon_a(\cdot)$ and $\varepsilon_p(\cdot)$ are the intrinsic amplitude and phase fluctuations, respectively. Note that in (1), the expression

$$\begin{aligned} p_r[n] &= \frac{A}{\sqrt{2}}\left[1+\varepsilon_a(t_r+nT_s)\right]\cdot e^{j\left[2\pi f_0(1+\zeta)t_r+\varepsilon_p(t_r+nT_s)+\phi\right]} = \\ &= \frac{A}{\sqrt{2}}\left[1+\varepsilon_{a_r}[n]\right]\cdot e^{j\left[\varepsilon_{p_r}[n]+\varphi_r\right]} \end{aligned} \quad (2)$$

denotes the waveform phasor referred to frequency $f_x = f_0(1+\zeta)$ at a generic sampling time $t_r+n\cdot T_s$, where $\varepsilon_{a_r}[n]=\varepsilon_a(t_r+nT_s)$ and $\varepsilon_{p_r}[n]=\varepsilon_p(t_r+nT_s)$ are the amplitude and phase fluctuation sequences and $\varphi_r = 2\pi f_0(1+\zeta)t_r+\phi$ is the phase at the reference time. Conversely, the synchrophasor $p_r'[n]$, as it is defined in the Standard [15], is referred to the nominal frequency f_0. The latter quantity is typically measured by a PMU at time t_r using a record of N samples. For the sake of simplicity we will assume in the following that T_s is constant and N is an odd number (however the case with N even can be addressed in a similar way). Thus, t_r lies exactly in the center of the observation interval, i.e. n=-(N-1)/2,…,(N-1)/2 in (2). The effect of possible sampling jitter will be described in Section VII. It is worth noticing that a digitized waveform processed by a PMU includes various disturbances. Therefore, it is not expressed by (1), but rather by

$$s_r[n] = x_r[n] + \varepsilon_{h_r}[n] + \varepsilon_{n_r}[n] \quad (3)$$

where $\varepsilon_{hr}[\cdot]$ includes all unwanted narrowband components (e.g. the first H harmonics along with other possible out-of-band interferers), and $\varepsilon_{nr}[\cdot]$ is additive wideband noise. Consider that phasor measurement uncertainty depends not only on various static or dynamic disturbances, but also on the chosen estimation algorithm. In particular, if phasors can be considered as *static* (i.e. approximately constant within each observation interval), the classic windowed DFT-based estimator is able to provide quite accurate results [25]. If instead phasors are regarded as *dynamic* (because they change significantly over time within the same observation interval), more sophisticated models including also the derivatives of phasors with respect to time are needed to achieve high accuracy [18], [19].

III. Static Phasor Estimator

If $\varepsilon_{a_r}[n]$ and $\varepsilon_{p_r}[n]$ in (2) are negligible, the waveform phasor can be regarded as *static* and, accordingly, $p_r[n]$ can be modeled as a constant p_{c_r}. In this case the windowed discrete-time Fourier transform (DTFT) of (3) in the rth observation interval is given by

$$S_{w_r}(\lambda) = \frac{\sqrt{2}}{N}\sum_{n=-\frac{N-1}{2}}^{\frac{N-1}{2}} s_r[n]\,w[n]\,e^{-j\frac{2\pi}{N}\lambda n} = X_{w_r}(\lambda) + \mathrm{E}_{h_r}(\lambda) + \mathrm{E}_{n_r}(\lambda) \quad (4)$$

where

$$X_{w_r}(\lambda) = p_{c_r}W(\lambda-\nu) + p_{c_r}^{*}W(\lambda+\nu), \quad (5)$$

λ and $\nu=f_x\cdot N\cdot T_s = (1+\zeta)\cdot N/M$ are the frequency variable and the fundamental frequency of (1), respectively, expressed in bins, * denotes the conjugate operator, and

$$W(\lambda) = \frac{1}{N}\sum_{n=-\frac{N-1}{2}}^{\frac{N-1}{2}} w[n]\,e^{-j\frac{2\pi}{N}\lambda n} \quad (6)$$

is the DTFT of the chosen window function $w[\cdot]$. The fundamental frequency in bins can be also rewritten as $\nu = C + \delta$, where C is the nominal integer number of observed cycles, and

$$\delta = \begin{cases} C \cdot \zeta & \text{if } C \cdot M \text{ is odd} \\ C \cdot \zeta + \frac{1+\zeta}{M} & \text{if } C \cdot M \text{ is even} \end{cases} \quad (7)$$

Observe that if $C \cdot M$ is an even number, an additional sample is added to the data record in order to process an odd number of samples N. If the Signal-to-Noise Ratio (SNR) is large enough, then $\mathrm{E}_{n_r}(\lambda)$ is negligible [11]. Moreover, if a sufficient number of waveform cycles is analyzed and if a suitable window is used, both the term $\mathrm{E}_{h_r}(\lambda)$ due the narrowband disturbances and the contribution of the image component $p^*_{c_r}$ at frequency $\lambda + \nu$ can be strongly reduced [25]. As a consequence, from (4) and (5) it follows that

$$S_{wr}(\lambda) \cong X_{wr}(\lambda) \cong p_{c_r} W(\lambda - \nu). \quad (8)$$

If typical cosine-class window functions are used, the spectrum peak of (3) is located at bin $\lambda = \nu$ and the phasor can be easily estimated from the Cth DFT sample, which is very close to this peak, i.e.

$$p_{c_r} \cong \frac{S_{w_r}(C)}{W(-\delta)}. \quad (9)$$

Observe that (9) totally neglects the influence of the image component and relies on the quantity δ, which is usually unknown. Nonetheless, if the window function exhibits a perfectly even symmetry with respect to the center of the observation interval, its transform is real-valued, so $\boldsymbol{Arg}\{W(\lambda)\} = 0$ for values of the normalized frequency λ inside the window spectrum main lobe. Thus

$$\boldsymbol{Arg}\{p_{c_r}\} \cong \boldsymbol{Arg}\{X_{w_r}(C)\}, \quad (10)$$

which shows that the phasor angle can be easily estimated, once the nominal integer number of observed cycles C is known. It is worth emphasizing that phasor magnitude and frequency estimation accuracy can be greatly improved by estimating δ through the Interpolated DFT (IpDFT) algorithm [29],[30]. The behavior of this static phasor estimator under possible impaired conditions in low-voltage distribution networks is analyzed in [31]. Performance can be enhanced by means of suitable window functions [32], or by compensating the spectral interference produced by the spectral leakage associated to the image of the fundamental tone [33]. However, if we limit our attention to phasor angle estimation only, there is no difference between the IpDFT and the basic DFT, provided that the observation interval is centered around the reference time. In this case, the window transform does not introduce a phase shift. For this reason, just the classic basic DFT-based phasor estimator will be used in the following comparison.

IV. Dynamic Phasor Estimators

As shortly explained in Section II, when a waveform phasor changes rapidly within the same observation interval, the static phasor model is no longer adequate for estimation purposes. In this situation, the waveform synchrophasor $p'_r[n]$ can be better described by its Taylor's series expansion around time t_r truncated to the Kth order term. As a result, (1) can be rewritten as

$$x_r[n] \cong \frac{\sqrt{2}}{2} \sum_{k=0}^{K} \left(n^k p_{r,k} e^{j\frac{2\pi}{M}(1+\zeta)n} + n^k p^*_{r,k} e^{-j\frac{2\pi}{M}(1+\zeta)n} \right) \quad (11)$$

where $p_{r,k} = \frac{1}{K!} p_r^{(k)}(t_r) \cdot T_s^k$, and $p_r^{(k)}(t_r)$ is the kth order derivative of (2) computed at time t_r. In the following, two recently proposed dynamic phasor estimators are recalled, i.e. the IpD^{2}FT algorithm [26] and the WTFF technique, as it is described in [27].

A. Interpolated Dynamic DFT (IpD^{2}FT) estimator

Assuming that in (3) both narrowband and wideband disturbances are negligible (i.e. $\varepsilon_{hr}[\cdot] \approx \varepsilon_{nr}[\cdot] \approx 0$), by replacing (11) into (4), the DTFT of the waveform acquired in the rth observation interval becomes

$$S_{w_r}(\lambda) \cong X_{w_r}(\lambda) \cong \sum_{k=0}^{K} p_{r,k} W_k(\lambda - \nu) + p^*_{r,k} W_k(\lambda + \nu) \quad (12)$$

where

$$W_k(\lambda) = \frac{1}{N} \sum_{n=-\frac{N-1}{2}}^{\frac{N-1}{2}} n^k w[n] e^{-j\frac{2\pi}{N}\lambda n} = \left(j\frac{N}{2\pi} \right)^k \frac{d^k W(\lambda)}{d\lambda^k} \quad (13)$$

Observe, that $W_0(\lambda)$ coincides with $W(\lambda)$. If the phasor Taylor's series is truncated to the second order (i.e., K=2) and the chosen window exhibits an even symmetry with respect to its central sample, the values of (12) for $\lambda = C+h$, h=1,0,-1, can be rearranged into the following linear system, i.e. [26]

$$\boldsymbol{S}_{w_r} \cong \boldsymbol{W_P}(\delta) \cdot \boldsymbol{P_r} + \boldsymbol{W_I}(\delta) \cdot \boldsymbol{P_r^*} \quad (14)$$

where

$$\boldsymbol{S}_{w_r} = \begin{bmatrix} S_{w_r}(C-1) \\ S_{w_r}(C) \\ S_{w_r}(C+1) \end{bmatrix} \quad \boldsymbol{P_r} = \begin{bmatrix} p_{r,0} \\ p_{r,1} \\ p_{r,2} \end{bmatrix} \quad \boldsymbol{P_r^*} = \begin{bmatrix} p^*_{r,0} \\ p^*_{r,1} \\ p^*_{r,2} \end{bmatrix} \quad (15)$$

and matrices

$$\boldsymbol{W_P}(\delta) = \begin{bmatrix} W_0(-1-\delta) & W_1(-1-\delta) & W_2(-1-\delta) \\ W_0(-\delta) & W_1(-\delta) & W_2(-\delta) \\ W_0(1-\delta) & W_1(1-\delta) & W_2(1-\delta) \end{bmatrix}, \quad (16)$$

$$\boldsymbol{W_I}(\delta) = \begin{bmatrix} W_0(2C-1+\delta) & W_1(2C-1+\delta) & W_2(2C-1+\delta) \\ W_0(2C+\delta) & W_1(2C+\delta) & W_2(2C+\delta) \\ W_0(2C+1+\delta) & W_1(2C+1+\delta) & W_2(2C+1+\delta) \end{bmatrix} \quad (17)$$

consist just of real elements. If δ is known, the real and the imaginary parts of vector $\boldsymbol{P_r}$ are given by

$$\begin{aligned} \boldsymbol{Re}\{\boldsymbol{P}_r\} &= [\boldsymbol{W_P}(\delta) + \boldsymbol{W_I}(\delta)]^{-1} \cdot \boldsymbol{Re}\{\boldsymbol{S}_{w_r}\} \\ \boldsymbol{Im}\{\boldsymbol{P}_r\} &= [\boldsymbol{W_P}(\delta) - \boldsymbol{W_I}(\delta)]^{-1} \cdot \boldsymbol{Im}\{\boldsymbol{S}_{w_r}\} \end{aligned}. \quad (18)$$

If δ is unknown instead (which is the most common case), the values of $\boldsymbol{P_r}$ can be obtained iteratively as follows. At first, δ in (16) and (17) is assumed to be equal to 0. Then, (18) is computed and the value of δ is obtained from (7), once the fractional frequency deviation ζ is estimated from [26]

$$\zeta = \frac{1}{2\pi M} \frac{\boldsymbol{Im}\{p_{r,1} p_{r,0}^*\}}{|p_{r,0}|^2}. \quad (19)$$

The new value of δ is then replaced into (18) and the same procedure is repeated till when the results of (19) do not change significantly. Indeed the convergence of the algorithm, which relies on a gradient-based approach (similarly to the classic Newton-Raphson method) is always guaranteed in the conditions specified in the Standards [15], [16], [28]. In fact, the frequency deviations are small enough to lie within the main lobe of the window spectrum and the chosen approach definitely converges to the wanted solution since no local minima exist. In particular, all simulations show that L = 2 or 3 iterations are enough to achieve accurate results. Thus, the phasor angle at time t_r is simply given by $\boldsymbol{Arg}\{p_{r,0}\}$.

B. Windowed Taylor-Fourier Filter (WTFF)

Let $\boldsymbol{x}_r$ be the column vector including all the samples of (1) collected in the rth observation interval under the assumption that narrowband and wideband disturbances are negligible (i.e. $\varepsilon_{hr}[\cdot] \approx \varepsilon_{nr}[\cdot] \approx 0$). In order to enable a fair comparison between the WTFF approach and the IpD^{2}FT algorithm, in the following, the Taylor series of (11) is truncated to the second order. If the elements of vectors $\boldsymbol{P_r}$ and $\boldsymbol{P_r^*}$ in (14) are rearranged in a single vector $\overline{\boldsymbol{P}}_r = \left[p_{r,2}^*, p_{r,1}^*, p_{r,0}^*, p_{r,0}, p_{r,1}, p_{r,2}\right]^T$ and

$$\Omega = \begin{bmatrix} w\left[-\frac{N-1}{2}\right] & 0 & \cdots & 0 \\ 0 & w\left[-\frac{N-1}{2}+1\right] & \cdots & 0 \\ \vdots & \vdots & \ddots & \vdots \\ 0 & 0 & \cdots & w\left[\frac{N-1}{2}\right] \end{bmatrix} \quad (20)$$

is referred to as the diagonal matrix built using the coefficients of the chosen window function, it is shown in [27] that the phasor in the rth observation interval, its first and second derivatives and the respective complex conjugate quantities can be estimated from

$$\overline{\boldsymbol{P}}_{\boldsymbol{r}} = 2\left(G^H \Omega^H \Omega G\right)^{-1} G^H \Omega^H \Omega \, \boldsymbol{x}_r \quad (21)$$

where ^{H} denotes the Hermitian operator and the N×6 matrix

$$G = \begin{bmatrix} G_1 & G_3 \\ G_2 & G_4 \end{bmatrix} \quad (22)$$

consists of four independent sub-matrices G_1, G_2, G_3 and G_4, whose individual elements are given by

$$\begin{aligned} (g_1)_{lq} &= \left(l - \frac{N-1}{2}\right)^{2-q} e^{j\left(\frac{N-1}{2}-l\right)\frac{2\pi}{M}}, \; l = 0,\ldots,\frac{N-1}{2} \text{ and } q = 0,1,2, \\ (g_2)_{lq} &= l^{2-q} e^{-jl\frac{2\pi}{M}}, \qquad\qquad l = 1,\ldots,\frac{N-1}{2} \text{ and } q = 0,1,2, \\ (g_3)_{lq} &= \left(l - \frac{N-1}{2}\right)^{q} e^{-j\left(\frac{N-1}{2}-l\right)\frac{2\pi}{M}}, \; l = 0,\ldots,\frac{N-1}{2} \text{ and } q = 0,1,2, \\ (g_4)_{lq} &= l^{q} e^{jl\frac{2\pi}{M}}, \qquad\qquad l = 1,\ldots,\frac{N-1}{2} \text{ and } q = 0,1,2. \end{aligned} \quad (23)$$

Observe that the coefficients in (23) are computed under the implicit assumption that the waveform frequency is equal to the nominal value f_0. Similarly to the case of the IpD^{2}FT algorithm, the angle of the estimated phasor at time t_r is extracted from $\overline{\boldsymbol{P}}_r$ by computing $\boldsymbol{Arg}\{p_{r,0}\}$.

V. Computational Complexity

As known, the evaluation of one DFT sample requires N complex products and N-1 complex additions. Therefore, complexity is $O(N)$, i.e. proportional to the number of collected samples. The complexity of the WTFF estimator is apparently larger, but the elements of matrix $2\left(G^H \Omega^H \Omega G\right)^{-1} G^H \Omega^H \Omega$ in (21) can be computed once and for all. As a consequence, the WTFF algorithm just relies on one row-column product in (21). Thus, it has the same computational complexity as the DFT-based approach. The complexity of the IpD^{2}FT algorithm is still linear with N, but it is larger than both DFT and WTFF estimators for various reasons, i.e. *i*) at least K+1 DFT samples of the transform of the acquired waveform have to be computed; ii) $2(K+1)^2$ samples of the window spectrum have to be evaluated to build matrices (16) and (17); iii) such matrices have to be inverted; iv) the algorithm is repeated L times and, finally, v) at the end of each iteration a new value of δ has to be estimated using (19) and (7). Evidently, the computational cost of the last operations for obtaining δ is negligible compared with the rest of the algorithm. Therefore, assuming that the number of iterations L is fixed, the order of complexity of the IpD^{2}FT estimator is approximately $O((K+1)\cdot N)+2L\cdot[O((K+1)^2\cdot N)+O((K+1)^3)]$, where the cubic rightmost term refers to the complexity of inverting a (K+1) X (K+1) matrix, using the Gauss–Jordan elimination technique. Even if the overall complexity of the IpD^{2}FT looks quite larger than the other solutions, in practice the values of both K and L are small (e.g. K=2 and L=3). Thus, the overall processing time to return a single phasor estimate is still dominated by the number of samples N, and it is just slightly than using a basic DFT estimator.

VI. Simulations Results

The accuracy of the phasor angle estimators described in Sections III and IV has been evaluated through extensive

Monte Carlo simulations in various conditions based on the Standards C37.118.1:2011 and EN 50160:2010 [15],[28]. Moreover, in order to test the accuracy of the phasor angle estimators described in Sections III and IV in transient conditions closer to those of distribution networks, some additional simulations under the influence of decaying DC offsets are reported at the end of this Section.

The choice of using two sets of testing conditions (and in some case their combination) is due to the fact that the Standard C37.118.1:2011 (along with its Amendment C37.118.1a:2014 [16]) deals with PMU performance regardless of how or where these instruments are used. On the contrary, the Standard EN 50160:2010 is specifically focused on the features of the voltage waveforms at the distribution level. In fact, as stated in the Introduction, active distribution networks are characterized by reduced line lengths, limited power flows and higher distortion levels than those of transmission networks [17].

Such features suggest that the PMU accuracy requirements at the distribution level are expected to be higher than those specified in the Standard C37.118.1:2011, although no phase measurement uncertainty limits are explicitly reported in [15] and [16]. In addition, at the distribution level the PMUs could be used to monitor electromechanical transients, which generally lead to non-negligible deviations from the nominal frequency. As a result, synchrophasors angles could be poorly estimated if waveform frequency changes within the chosen observation intervals are too relevant to be accurately measured.

All simulations rely on some common assumptions, which are shortly listed below.

- The reference time at which every phasor is computed is located in the center of the considered observation interval.
- The number of samples per nominal waveform cycle M is set equal to 129. However, results are almost independent of record size if the Nyquist theorem is satisfied.
- All observation intervals consist of an odd number of samples and include approximately an integer number of waveform cycles, ranging from C=2 to C=6.
- Various B-term *Maximum Side-lobe level Decay* (MSD) cosine windows (with B = 2, 3, 4) are used in all cases, as they proved to be effective in heterogeneous conditions [34].
- In every simulation run, the phases of fundamental tone, harmonics and modulating signals (if present) at the reference time are chosen at random in $[0,2\pi)$. In particular, 100 waveforms with random phase values are used for each value of the fractional frequency deviation ζ.
- three iterations of the IpD^{2}FT algorithm are considered since a greater number of iterations does not improve results significantly.

The absolute values of the maximum phase errors associated with the DFT, IpD^{2}FT and WTFF estimation algorithms are shown in Tables I, II and III, respectively. All data are expressed in mrad and refer orderly to the conditions summarized below, i.e.:

a) Pure sine-wave affected by a fractional static off-nominal frequency deviation ζ changing linearly in the range [-0.1,0.1], in compliance with the worst-case requirements of the Standard IEEE C37.118.1:2011 (*case a*).
b) Sine-wave with static frequency deviation ζ changing linearly in the range [-0.1,0.1] and affected by a 40-dB Signal-to-Noise Ratio (SNR) due to zero-mean additive wideband Gaussian noise (AWGN) (*case b*); 500 noisy realizations for every waveform phase are used in this case.
c) Waveform with a fundamental tone static frequency deviation ζ in the range [-0.1,0.1] and perturbed by a 2nd-order harmonic (*case c*) of amplitude equal to 10% of the fundamental, as recommended for *M-Class* compliance in [15].
d) Waveform with a fundamental tone static frequency deviation ζ in the range [-0.1,0.1] and perturbed by a 3rd-order harmonic (*case d*) of amplitude equal to 10% of the fundamental, as recommended for *M-Class* compliance in [15].
e) Waveform with a fundamental tone static frequency deviation ζ in the range [-0.1,0.1] and perturbed by all harmonics till the 25th; each harmonic amplitude is compliant with the worst-case specified in the Standard EN 50160:2010 [28] (*case e*).
f) Waveform with a fundamental tone static frequency deviation ζ in the range [-0.1,0.1] and affected by sinusoidal amplitude modulation (AM) with amplitude 10% of the fundamental and frequency equal to $0.1 \cdot f_0$, according with the worst case reported in [15] (*case f*);
g) Waveform with a fundamental tone static frequency deviation ζ in the range [-0.1,0.1] and affected by joint sinusoidal amplitude and phase modulations (AM+PM) with amplitude equal to 10% of the fundamental and 0.1 rad for AM and PM, respectively, and frequency equal to $0.1 \cdot f_0$, according with the worst case conditions reported in the [15] (*case g*).
h) *Case h* results from the superposition of the disturbances described in *case e* and *case g*.
i) In *case i* a sine-wave at nominal frequency is perturbed by an out-of-band sinusoidal interferer with magnitude equal to 10% of the fundamental, phase chosen randomly in $[0, 2\pi)$ and frequency equal to 10 Hz, 25 Hz, 75 Hz or 100 Hz, assuming a reporting rate (*RR*) equal to 50 fps [15].
j) In *case j* the fundamental frequency is assumed to be nominal, but the collected waveform is affected by an amplitude step of magnitude equal to ±10% of the nominal value.
k) Finally, in case *k* the fundamental frequency is assumed to be nominal, but the collected waveform is affected by a phase step of ±10° (i.e. $\pm\pi/18$), according with the worst-case conditions reported in [15].

The results reported in Tables I, II and III show that:

- in the case of static off-nominal frequency deviations only (i.e. *case a*), the IpD^{2}FT method is slightly better than the WTFF approach and both techniques outperform the DFT-based estimator.

TABLE I – MAXIMUM ABSOLUTE VALUES OF THE PHASE ESTIMATION ERRORS (EXPRESSED IN mrad) OBTAINED WITH THE CLASSIC DFT-BASED PHASOR ESTIMATION ALGORITHM IN DIFFERENT TESTING CONDITIONS. 2-, 3- OR 4-TERM MSD WINDOWS OVER OBSERVATION INTERVALS WITH A DURATION BETWEEN ABOUT 2 AND 6 WAVEFORM CYCLES.

Case	Test conditions	Max [mrad]	2-term MSD			3-term MSD			4-term MSD		
			$C=2$	$C=3$	$C=4$	$C=3$	$C=4$	$C=5$	$C=4$	$C=5$	$C=6$
a	Freq. dev. only $[-10\%, 10\%]$[1]	|err.|	3.5	1.5	0.8	0.2	0.1	0.0	0.0	0.0	0.0
b	Freq. dev. $[-10\%, 10\%]$[1] + noise (SNR=40 dB)	|err. bias|	0.1	0.1	0.1	0.1	0.1	0.1	0.1	0.1	0.1
		err. std. dev.	1.3	1.1	0.7	0.7	0.7	0.6	0.7	0.6	0.6
c	Freq. dev.+2^{nd} harm. (10%)[1]	|err.|	15.6	4.3	1.5	6.4	0.5	0.1	3.0	0.1	0.0
d	Freq. dev.+3^{rd} harm. (10%)[1]	|err.|	4.3	1.5	0.8	0.2	0.1	0.0	0.0	0.0	0.0
e	Freq. dev.+25 harm. (10%)[2]	|err.|	5.8	2.0	0.9	1.4	0.1	0.0	0.6	0.0	0.0
f	Freq. dev.+AM[1]	|err.|	8.5	12.8	19.9	7.2	12.2	18.5	8.8	13.5	19.0
g	Freq. dev.+AM[1]+PM[1]	|err.|	10.4	16.8	28.2	10.3	17.8	26.5	13.0	19.4	26.6
h	Freq. dev.+AM[1]+PM[1]+25 harm.[2]	|err.|	13.6	17.8	28.8	11.4	17.7	26.6	13.3	19.1	27.1
i	10% out-of-band interferers[1]	|err.|	50.0	17.3	0.8	38.9	16.5	4.3	29.9	14.1	5.0
j	10% magnitude step[1]	|err.|	8.1	5.2	3.9	6.9	5.1	4.1	6.2	4.9	4.1
k	10° phase step[1]	|err.|	102	96.4	94.0	99.4	96.2	94.4	98.1	95.9	94.4

TABLE II – MAXIMUM ABSOLUTE VALUES OF THE PHASE ESTIMATION ERRORS (IN mrad) OBTAINED WITH THE IPD^{2}FT PHASOR ESTIMATION ALGORITHM FOR K=2 IN DIFFERENT TESTING CONDITIONS. 2-, 3- OR 4-TERM MSD WINDOWS OVER OBSERVATION INTERVALS WITH A DURATION BETWEEN ABOUT 2 AND 6 WAVEFORM CYCLES.

Case	Test conditions	Max [mrad]	2-term MSD			3-term MSD			4-term MSD		
			$C=2$	$C=3$	$C=4$	$C=3$	$C=4$	$C=5$	$C=4$	$C=5$	$C=6$
a	Freq. dev. only $[-10\%, 10\%]$[1]	|err.|	0.0	0.0	0.0	0.0	0.0	0.0	0.0	0.0	0.0
b	Freq. dev. $[-10\%, 10\%]$[1] + noise (SNR=40 dB)	|err. bias|	0.1	0.1	0.1	0.1	0.1	0.1	0.1	0.1	0.1
		err. std. dev.	1.1	0.9	0.8	1.0	0.9	0.8	0.9	0.9	0.8
c	Freq. dev.+2^{nd} harm. (10%)[1]	|err.|	71.9	21.9	2.8	46.9	12.6	0.6	28.7	7.6	0.4
d	Freq. dev.+3^{rd} harm. (10%)[1]	|err.|	2.8	0.4	0.2	0.1	0.0	0.0	0.0	0.0	0.0
e	Freq. dev.+25 harm. (10%)[2]	|err.|	15.7	4.4	0.6	9.4	2.5	0.1	5.7	1.5	0.1
f	Freq. dev.+AM[1]	|err.|	2.1	0.8	1.0	0.3	0.5	1.1	0.3	0.7	1.4
g	Freq. dev.+AM[1]+PM[1]	|err.|	2.1	0.8	1.2	0.3	0.6	1.4	0.4	0.8	1.7
h	Freq. dev.+AM[1]+PM[1]+25 harm.[2]	|err.|	16.4	5.2	1.6	10.4	3.1	1.4	6.3	2.3	1.7
i	10% out-of-band interferers[1]	|err.|	98.3	73.9	43.3	85.4	64.3	39.2	75.6	55.2	34.4
j	10% magnitude step[1]	|err.|	14.9	9.5	7.2	12.6	9.1	7.1	10.6	8.3	6.9
k	10° phase step[1]	|err.|	117	105	100	109	103	100	106	102	99.2

TABLE III – MAXIMUM ABSOLUTE VALUES OF THE PHASE ESTIMATION ERRORS (EXPRESSED IN mrad) OBTAINED WITH THE WTFF PHASOR ESTIMATION ALGORITHM FOR K=2 IN DIFFERENT TESTING CONDITIONS. 2-, 3- OR 4-TERM MSD WINDOWS OVER OBSERVATION INTERVALS WITH A DURATION BETWEEN ABOUT 2 AND 6 WAVEFORM CYCLES.

Case	Test conditions	Max [mrad]	2-term MSD			3-term MSD			4-term MSD		
			$C=2$	$C=3$	$C=4$	$C=3$	$C=4$	$C=5$	$C=4$	$C=5$	$C=6$
a	Freq. dev. only $[-10\%, 10\%]$[1]	|err.|	0.6	0.0	0.0	0.2	0.0	0.0	0.0	0.0	0.0
b	Freq. dev. $[-10\%, 10\%]$[1] + noise (SNR=40 dB)	|err. bias|	0.1	0.1	0.1	0.1	0.1	0.1	0.1	0.1	0.1
		err. std. dev.	1.2	1.0	0.8	1.1	0.9	0.8	1.0	0.9	0.8
c	Freq. dev.+2^{nd} harm. (10%)[1]	|err.|	84.9	38.2	6.3	67.3	35.6	12.4	55.4	30.6	12.6
d	Freq. dev.+3^{rd} harm. (10%)[1]	|err.|	3.1	0.3	0.0	1.0	0.0	0.0	0.2	0.0	0.0
e	Freq. dev.+25 harm. (10%)[2]	|err.|	17.4	7.7	1.3	13.6	7.1	2.5	11.2	6.1	2.5
f	Freq. dev.+AM[1]	|err.|	0.8	0.4	1.0	0.3	0.4	0.9	0.2	0.5	0.9
g	Freq. dev.+AM[1]+PM[1]	|err.|	1.1	0.6	1.8	0.5	0.7	1.7	0.4	0.9	1.8
h	Freq. dev.+AM[1]+PM[1]+25 harm.[2]	|err.|	18.4	8.7	3.0	14.9	8.2	3.3	12.3	7.2	3.6
i	10% out-of-band interferers[1]	|err.|	107	83.6	59.1	96.8	80.4	63.0	89.9	77.1	61.9
j	10% magnitude step[1]	|err.|	20.7	11.6	8.4	16.6	11.5	9.0	14.3	11.0	9.0
k	10° phase step[1]	|err.|	122	107	102	116	107	103	112	107	103

[1]Conditions compliant with the requirements of the Standard IEEE C.37.118.1:2011.
[2]Conditions compliant with the requirements of the Standard EN 50160:2010.

- However, the maximum phase errors associated with any algorithms can be made negligible by increasing the observation interval length. Such results are basically the same as those obtained by changing linearly ζ at a rate of 1 Hz/s, as described in the case of ramp testing in [15] and [16], since this rate of change of frequency produces very small frequency changes when considering short observation intervals.
- In the presence of noise (i.e. *case b*) the DFT-based estimator provides the best accuracy, while the dynamic estimators exhibit similar performances. Also, the standard deviations of the estimation is reduced by using longer observation intervals.
- The classic DFT-based approach is generally less sensitive to harmonics than the IpD^{2}FT estimator, which in turn performs better than the WTFF algorithm (*cases c*, *d* and *e*). The higher sensitivity of the dynamic approaches to harmonics is mainly due to the use of phasor derivatives. Again, in all cases considered the maximum phase errors can be reduced by increasing the observation interval

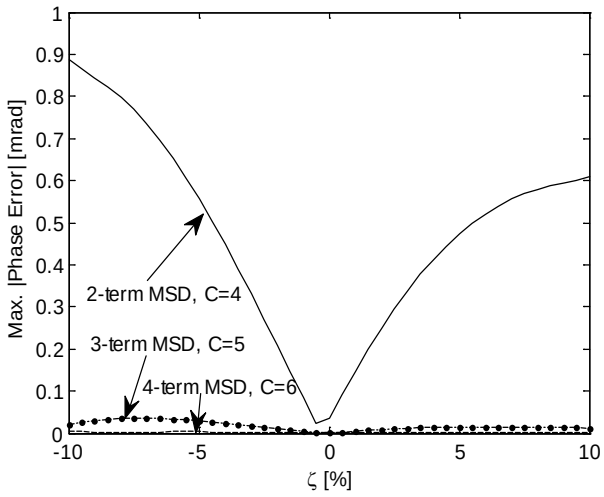

(a)

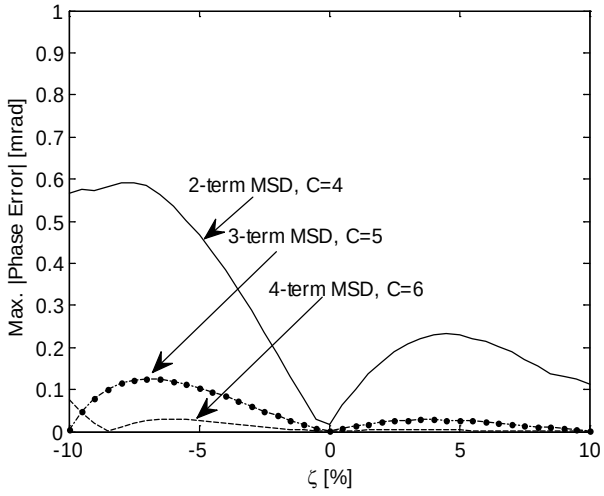

(b)

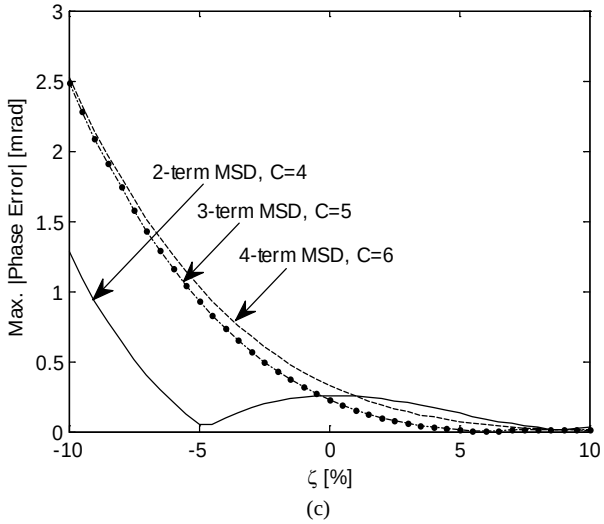

(c)

Fig. 1 – Maximum absolute values of the phase estimation errors associated with the classic DFT-based technique (a), the IpD^{2}FT algorithm (b), and the WTFF estimator (c), as a function of the static off-nominal frequency deviation ζ and under the effect of a worst-case total harmonic distortion compliant with the Standard EN 50160:2010.

length.

Under the effect of amplitude and/or phase modulation (i.e. *cases f* and *g*), both the WTFF technique and the IpD^{2}FT algorithm outperform the classic DFT-based estimator, as expected, since they take advantage of the dynamic phasor model. However, unlike the previous cases, the accuracy of all techniques degrades when *C* grows. This is quite intuitive because phasor changes are smoothed by longer intervals.

- The considerations above suggest that, in the presence of both steady-state harmonic distortion and modulations (*case h*), for a given type of window, the best accuracy is achieved as a tradeoff between opposite trends. This is not clearly visible from Tables I-III, since, with the chosen values of *C*, the effect of harmonics prevails over modulations. As a consequence, the maximum phase errors for a given number of window terms *B*, apparently decrease monotonically. However, further simulations confirm that, the phase error values exhibit a growing trend as soon as, by increasing *C*, the effect of modulations prevails over harmonic distortion.
- When a large out-of-band interferer is close to the fundamental tone (*case i*) the phase errors associated with all estimators become quite large. However, the DFT estimator is much less sensitive to the out-of-band interferers than the IpD^{2}FT algorithm. In turn, this is less sensitive than the WTFF estimator. Also, accuracy improves as the observation interval length increases since the frequency distance between the fundamental component and the interfering tone increases.
- The last two rows of all Tables report the maximum phase errors associated with the three estimators in transient conditions, i.e. under the effect of amplitude steps (*case j*) or phase steps (*case k*), respectively. The DFT estimator is less sensitive to transients than the IpD^{2}FT algorithm. This, however, performs clearly better than the WTFF. As expected, the maximum error due to a phase step is much larger than the maximum error related to a magnitude step, as the former impacts directly on the phase of the waveform. Observe that in all the considered cases the errors tend to decrease, even if slowly, as the observation interval length grows.

When the IpD^{2}FT algorithm is considered, the number of terms of the Taylor's series deserves a special attention. Indeed, if *K* increases (e.g. *K*=3), the observation interval length has to increase as well to avoid significant spectral interferences due to other spectral components such as harmonics or the image tone. As a result, the IpD^{2}FT algorithm responsiveness degrades, but accuracy tends to slightly improve by using *K*=3 rather than *K*=2. However, by increasing *K* the algorithm becomes more sensitive to wideband noise (i.e. in *case b*). Ultimately, *K*=2 provides a good tradeoff between overall accuracy and responsiveness.

In Fig. 1 the maximum absolute values of the phase estimation errors associated with the DFT-based technique (a), the IpD^{2}FT algorithm (b), and the WTFF estimator (c), respectively, are compared in the testing conditions related to *case e*. The error curves are plotted as a function of ζ for

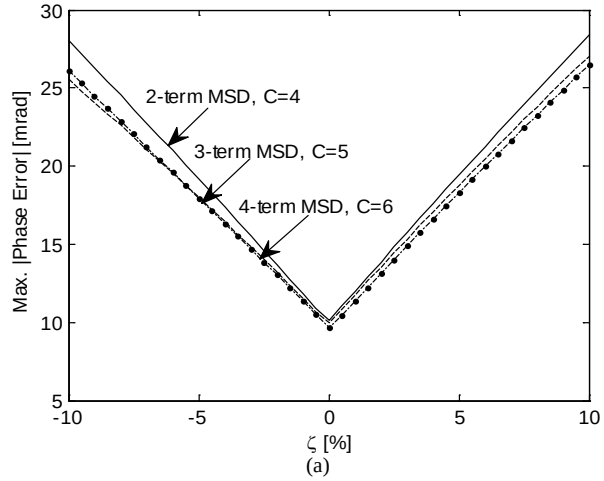

(a)

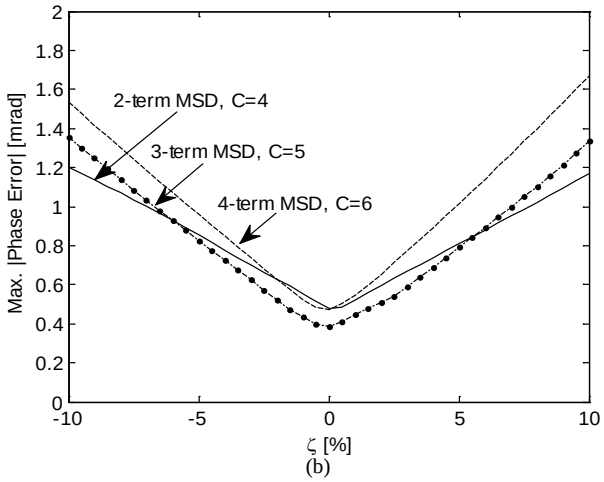

(b)

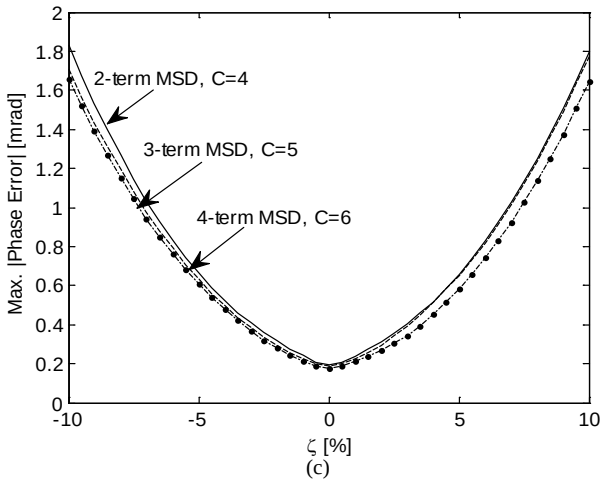

(c)

Fig. 2 – Maximum absolute values of the phase estimation errors associated with the DFT-based technique (a), the IpD^{2}FT algorithm (b), and the WTFF estimator (c), under the joint effect of: static off-nominal frequency deviations $\zeta \neq 0$, amplitude modulation (AM) and phase modulation (PM). The modulating signals are two sine-waves of amplitude equal to 10% of the fundamental and 0.1 rad for AM and PM, respectively, and frequencies equal to $0.1 \cdot f_0$.

C=*B*+2 cycles when a *B*-term MSD window is used (with *B* = 2, 3 or 4). The plots confirm that the DFT-based solution is slightly more robust to harmonics than the others. However, the WTFF estimator can be significantly affected by harmonics when ζ is negative.

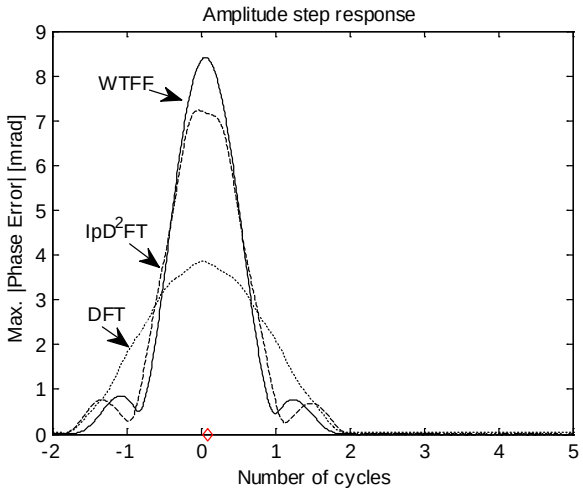

(a)

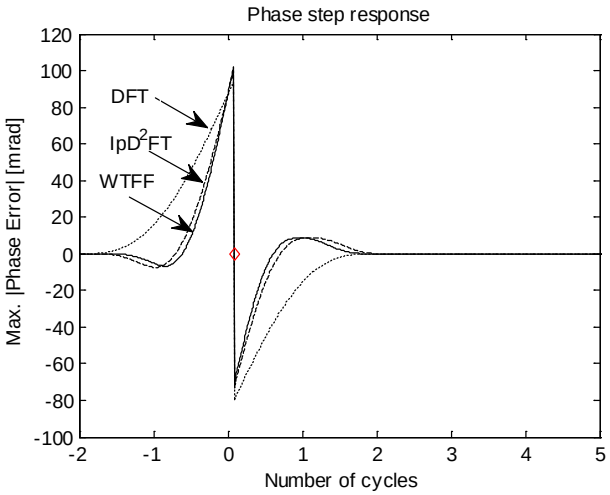

(b)

Fig. 3 – Phase errors envelopes as a function of time (expressed in nominal waveform cycles) when either a 10% magnitude step (a) or a 10° phase step occurs (b). Different line styles refer to the DFT-based technique, the IpD^{2}FT algorithm and the WTFF estimator, when a 2-term MSD window is used over a four-cycle observation interval. The small diamonds highlight when the step occurs.

Fig. 2 shows the maximum absolute values of the phase estimation errors associated with the DFT-based technique (a), the IpD^{2}FT algorithm (b), and the WTFF estimator (c), under the testing conditions related to the *case g*. The adopted windows and the observation interval lengths are the same as those used in Fig. 1. However, in this case the IpD^{2}FT algorithm and the WTFF estimator clearly outperform the classic DFT-based approach.

Fig. 3(a)-(b) provides an example of the transient behavior of all the analyzed estimators under the testing conditions related to the *cases j* and *k*, respectively. In Fig. 3(a)-(b) the maximum phase error envelopes associated with the three estimators are plotted as a function of time expressed in nominal waveform cycles, when the observation interval is about *C*=4 cycles long and a 2-term MSD window is used.

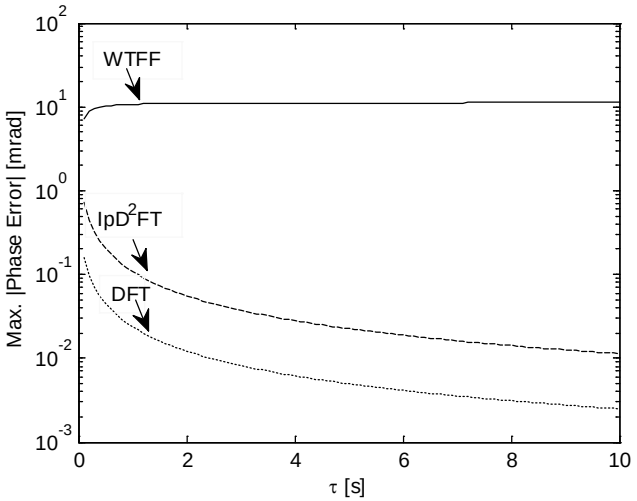

Fig. 4 - Maximum phase errors as a function of the time constant of an additive decaying DC offset of initial amplitude equal to 70% of the nominal waveform amplitude. Different line styles refer to the DFT-based technique, the IpD^{2}FT algorithm and the WTFF estimator, respectively, when a 3-term MSD window is used over a five-cycle-long observation interval.

The curves confirm that when a amplitude step occurs the maximum error introduced by the DFT-based estimator is generally smaller than the maximum error associated with the IpD^{2}FT algorithm or by the WTFF technique. Conversely, in the presence of phase steps, errors are much larger and quite similar. Quite interestingly, the duration of transients is almost the same for all estimators in both *case j* and *case k*. Additional simulation results, not reported for the sake of brevity, show that the error peaks during transients are almost proportional to the step size, both in magnitude or in phase.

Since the effect of transients is particularly interesting in the case of distribution networks, some additional results under the influence of decaying DC offsets (not included in the Standards considered) are reported in Fig. 4. The three curves displayed with different line styles represent the maximum phase errors associated with the three considered estimators, when the observation interval is C=5 cycles long and a 3-term MSD window is used. In all cases, exponentially decreasing DC offsets with initial amplitude equal to 70% of the fundamental and time constant τ in the range between 0.1 and 10 s are added to a sinusoidal voltage waveform of frequency f_0 [33]. Each point of the curves is the maximum phase error resulting from 200 initial phase values chosen at random in $[0,2\pi)$. The decaying DC offset always start at the beginning of the observation intervals. The reported results show that the DFT approach is the least sensitive to the influence of such disturbances. Accuracy is about one order of magnitude worse for the IpD^{2}FT algorithm and at least two orders of magnitude worse with the WTFF estimator. By changing the observation interval length or the type of window, similar patterns are obtained. Observe that the phase errors associated with the DFT and IpD^{2}FT estimators exhibit a monotonically decreasing trend. This is due to the fact that when τ grows, the spectral content of the decaying DC offsets is increasingly concentrated around zero, i.e. faraway from the spectral samples used by the algorithms. On the contrary, the sensitivity of the WTFF estimator to decaying DC offsets is not only larger, but it is also almost independent of the values of τ. This is due to the fact that the WTFF estimator relies on the weighted least square fitting in the time domain of a dynamic (i.e. oscillating) phasor model, which does not include any decaying DC offset. Therefore, such terms cannot be tracked with good accuracy regardless of the value of τ.

VII. Jitter and Time Alignment Uncertainty

The analysis performed in the previous Sections was focused on the effect of phasor estimation algorithms only. However, as stated in the Introduction, additional uncertainty contributions arise from: i) sampling jitter, ii) limited synchronization accuracy, and iii) the need to estimate the phase of a waveform at times different from the center of the considered observation interval. The sampling jitter depends on the fact that even if the sampling clock is disciplined by a GPS receiver or by some other synchronization technique (e.g. the IEEE 1588 Precision Time Protocol [35]), the input waveform within the rth observation interval is actually sampled at times which slightly differ from t_r+nT_s. If we denote with δ_{T_s} the random time fluctuations of the sampling period T_s, the equivalent effect of this term on phasor estimation algorithms is to inject an additional phase modulation term in the signal model. This means that $\varepsilon_{p_r}[n]$ in (2) should be rather replaced by $\varepsilon'_{p_r}[n]=\varepsilon_{p_r}[n]+2\pi\sum_{i=0}^{n}\delta_{T_s}[i]$. In addition, because of the limited synchronization accuracy, even if the delays due to the acquisition stage are properly estimated and compensated, the phase in the center of the considered observation interval is affected by some uncertainty. In particular, if t_j models the synchronization uncertainty, then the corresponding phase uncertainty at reference time t_r can be approximated by a first-order Taylor series expansion as follows:

$$\Delta\varphi_{j_r}=\left(2\pi f_0(1+\zeta)+\left.\frac{d\varepsilon_p}{dt}\right|_{t=t_r}\right)t_j\,. \qquad (24)$$

In practice, the values of t_j usually range from some hundreds of ns to a few μs. For instance, if the worst-case synchronization uncertainty is 1 μs, the absolute value of the maximum phase error $\Delta\varphi_{j_{max}}$ returned by (24) is about 0.4 mrad, i.e. smaller than (or at most comparable to) the algorithm-related phasor estimation errors in most of the conditions considered.

A further uncertainty contribution affecting phasor angle measurements arises from the need to reconstruct the phasor data at times different from the reported ones. In fact, the PMU reporting rate depends on various factors, such as the performance class of the instrument (i.e. *P-class* or *M-class* [15]), the specific features of the PMU employed and the chosen instrument settings. When multiple streams of data are collected by a Phasor Data Concentrator (PDC) at different rates, all measurements need to be aligned in time. In such cases, the phasor angle φ_r' at a generic time $t_r' = t_r + \Delta t$ results

approximately from [23]

$$\varphi_r' \cong \varphi_r + 2\pi\left[(f_r - f_0)\Delta t + \frac{\Delta t^2}{2} ROCOF_r\right], \qquad (25)$$

where φ_r, f_r and $ROCOF_r$ are the phase, the frequency and the ROCOF values at time t_r. In practice, both f_r and $ROCOF_r$ are affected by some uncertainty that propagates to the phase estimate. If we denote with FE_r and RFE_r the frequency and ROCOF measurement errors in the rth observation interval, it results immediately from (25) that the phase error due to time alignment is:

$$\Delta\varphi_{a_r} = 2\pi\left(FE_r \cdot \Delta t + \frac{\Delta t^2}{2} \cdot RFE_r\right). \qquad (26)$$

In [23] it is noticed that the maximum FE and RFE values in the steady-state conditions reported in the Standard IEEE C37.118.1:2011 are too strict for *P-class* instruments and too loose for *M-class* PMUs. In fact, new and more sensible limits have been recently published in an Amendment to the same Standard [16]. In steady-state conditions (namely in the presence of off-nominal frequency deviations, harmonics and/or out-of-band interferers) the new FE and RFE upper bounds for *P-class* PMUs are 0.005 Hz and 0.4 Hz/s, respectively. In the case of *M-class* instruments instead, the scenario is more complex as the maximum FE values are 0.0025 Hz, 0.005 Hz, or 0.01 Hz depending on the considered testing condition, while the RFE limit is specified only in the off-nominal case (0.1 Hz/s). In dynamic conditions (particularly, when significant amplitude or phase modulations occur), depending on the PMU reporting rate, the FE and RFE limits lie in the following intervals: [0.03,0.06] Hz and [0.6,2.3] Hz/s, respectively, for a *P-class* PMU and [0.12,0.30] Hz and [2.3,14] Hz/s for an *M-class* PMU. By replacing in (26) the maximum values reported above and noticing that the time misalignment Δt could be up to 70 ms for a *P-class* PMU, or up to 300 ms for an *M-class* PMU [23], it follows immediately that the worst-case phase errors $\Delta\varphi_{a_{\max}}$ are:

- up to about 8 mrad in steady-state conditions and up to about 62 mrad in dynamic conditions when considering *P-Class* PMUs;
- up to about 47 mrad in steady-state conditions and between about 350 mrad (fast reporting rates) to about 876 mrad (slow reporting rates) under the effect of modulations for *M-Class* PMUs.

Thus, the time alignment uncertainty may quickly become the main contributor to the overall phase error.

VIII. Conclusion

In this paper the phase measurement accuracy of three different phasor estimators (i.e. the classic DFT-based algorithm, the Interpolated Dynamic DFT algorithm (IpD^{2}FT) and the Windowed Taylor-Fourier Filter (WTFF)) are compared in various conditions reported in the Standards IEEE C37.118.1:2011, IEEE C37.118.1a:2014 and EN 50160:2010. Using a common set of window functions and observation intervals, it turns out that the classic DFT-based estimator is less sensitive to harmonics, out-of-band interferers, amplitude or phase steps. The IpD^{2}FT and WTFF estimators instead are particularly accurate in the presence of waveform amplitude and/or phase fluctuations. While the WTFF technique is globally slightly better in dynamic conditions, the IpD^{2}FT algorithm exhibits a lower sensitivity to steady-state disturbances, step-like changes and decaying DC offsets. Apparently, no estimator is able to provide the best results in all situations. In addition, the accuracy of all the considered methods can be strongly affected by quick frequency or phase variations, as it may happen during transients. Finally, it is worth emphasizing that even though sampling and synchronization jitter have usually a minor impact on the overall phase error, possible time misalignments between the results returned by different PMUs (e.g. due to frequency and ROCOF limited measurement accuracy) could lead to intolerably large phase errors.

References

[1] A. Moschitta, P. Carbone, C, Muscas, "Performance Comparison of Advanced Techniques for Voltage Dip Detection," *IEEE Trans. on Instrumentation and Measurement*, vol.61, no. 5, pp. 1494-1502, May 2012.

[2] L. Peretto, "The Role of Measurements in the Smart Grid Era," *IEEE Instr. & Meas. Magazine*, vol. 13, no. 3, pp. 22-25, Jun. 2010.

[3] D. Carty, M. Atanacio, "PMUs and their Potential Impact on Real-time Control Center Operations," Proc. *IEEE Power and Energy Society General Meeting*, Minneapolis, MN, USA, pp. 1-3, Jul. 2010.

[4] J. Sexauer, P. Javanbakht, S. Mohagheghi, "Phasor Measurement Units for the Distribution Grid: Necessity and Benefits," Proc. *Innovative Smart Grid Technologies (ISGT)*, Copenaghen, Denmark, pp. 1-6, Feb. 2013.

[5] A. Borghetti, C.A. Nucci, M. Paolone, G. Ciappi, A. Solari, "Synchronized Phasors Monitoring During the Islanding Maneuver of an Active Distribution Network," *IEEE Trans. on Smart Grid*, vol. 2, no. 1, pp. 82-91, Mar. 2011.

[6] D. Feng, C.D. Booth, "Protection and Stability Assessment in Future Distribution Networks using PMUs," Proc. *Int. Conf. Developments in Power Systems Protection* (DPSP), Birmingham, UK, pp. 1-6, Apr. 2012.

[7] M. Pau, P.A. Pegoraro, S. Sulis, "Efficient Branch-Current-Based Distribution System State Estimation Including Synchronized Measurements," *IEEE Trans. on Instrumentation and Measurement*, vol. 62, no. 9, pp. 2419-2429, Sep. 2013.

[8] R.A.F. Pereira, L.G.W. Da Silva, J.R.S. Mantovani, "PMUs Optimized Allocation using a Tabu Search Algorithm for Fault Location in Electric Power Distribution System," Proc. *Transmission and Distribution Conference and Exposition: Latin America, IEEE/PES*, Sao Paulo, Brazil, pp. 143-148, Nov. 2004.

[9] A. Carta, N. Locci, C. Muscas, "GPS-Based System for the Measurement of Synchronized Harmonic Phasors," *IEEE Trans. on Instrumentation and Measurement*, vol. 58, no. 3, pp. 586-593, Mar. 2009.

[10] I. Cvetkovic, T. Thacker, D. Dong, G. Francis, V. Podosinov, D. Boroyevich, F. Wang, R. Burgos, G. Skutt, J. Lesko, "Future Home Uninterruptible Renewable Energy System with Vehicle-to-grid Technology," Proc. *Energy Conversion Congress and Exposition* (ECCE), San Jose, CA, USA, pp. 2675-2681, Sep. 2009.

[11] G. Barchi, D. Macii, D. Petri, "Synchrophasor Estimators Accuracy: a Comparative Analysis," *IEEE Trans. on Instrumentation and Measurement*, vol. 62, no. 5, pp. 963-973, May 2013.

[12] G. Barchi, D. Macii, D. Belega, D. Petri, "Performance of Synchrophasor Estimators in Transient Conditions: A Comparative Analysis," *IEEE Trans. on Instrumentation and Measurement*, vol. 62, no. 9, pp. 2410-2418, Sep. 2013.

[13] M. Wache, D. C. Murray, "Application of Synchrophasor Measurements for Distribution Networks," Proc. *Power and Energy Society General Meeting*, Detroit, MI, USA, pp. 1-4, Jul. 2011.

[14] L.F. Ochoa, D.H. Wilson, "Angle Constraint Active Management of Distribution Networks with Wind Power," Proc. *Innovative Smart Grid Technologies Conference Europe*, Gothenburg, Sweden, pp. 1-5, Oct. 2010.

[15] IEEE Standard C37.118.1-2011, *IEEE Standard for Synchrophasor Measurements for Power Systems*.

[16] IEEE Standard C37.118.1a-2014 (Amendment to IEEE Std C37.118.1-2011) *IEEE Standard for Synchrophasor Measurements for Power Systems -- Amendment 1: Modification of Selected Performance Requirements*, pp. 1-25, Apr. 2014.

[17] M. Paolone, A. Borghetti, C.A. Nucci, "A synchrophasor estimation algorithm for the monitoring of active distribution networks in steady state and transient conditions," Proc. *Power Systems Computation Conference* (PSCC), Stockholm, Sweden, pp. 1-6, Aug. 2011.

[18] W. Premerlani, B. Kasztenny, M. Adamiak, "Development and Implementation of a Synchrophasor Estimator Capable of Measurements Under Dynamic Conditions," *IEEE Trans. on Power Delivery*, vol. 23, no. 1, pp. 109-123, Jan. 2008.

[19] J. A. de la O Serna, "Dynamic Phasor Estimates for Power System Oscillation," *IEEE Trans. on Instrumentation and Measurement*, vol. 56, no. 5, pp. 1648-1657, Oct. 2007.

[20] A. von Meier, D. Culler, A. McEachern, and R. Arghandeh, "Microsynchrophasors for distribution systems," in *IEEE PES Innovative Smart Grid Technologies Conference* (ISGT), Washington DC, USA, pp. 1–5, Feb. 2014.

[21] IEEE Standard C57.13-1993, *IEEE standard requirements for instrument transformers*.

[22] P. Ferrari, A. Flammini, S. Rinaldi, G. Prytz, "Evaluation of Time Gateways for Synchronization of Substation Automation Systems," *IEEE Trans. Instrumentation and Measurement*, vol. 61, no. 10, pp. 2612-2621, Oct. 2012.

[23] A. J. Roscoe, I. F. Abdulhadi, G.M. Burt, "P and M Class Phasor Measurement Unit Algorithms Using Adaptive Cascaded Filters," *IEEE Trans. on Power Delivery*, vol. 28, no. 3, pp. 1447-1459, Jul. 2013.

[24] G. Barchi, D. Fontanelli, D. Macii, D. Petri, "Frequency-domain Phase Measurement Algorithms for Distribution Systems," Proc. *IEEE Int. Instrumentation and Measurement Technology Conference* (I2MTC), Montevideo, pp. 102-107, Uruguay, May 2014.

[25] D. Macii, D. Petri, A. Zorat, "Accuracy Analysis and Enhancement of DFT-Based Synchrophasor Estimators in Off-Nominal Conditions," *IEEE Trans. on Instrumentation and Measurement*, vol. 61, no. 10, pp. 2653-2664, Oct. 2012.

[26] D. Petri, D. Fontanelli, D. Macii, "A Frequency-Domain Algorithm for Dynamic Synchrophasor and Frequency Estimation," *IEEE Transactions on Instrumentation and Measurement*, vol. 63, no. 10, pp. 2330-2340, Oct. 2014.

[27] M.A. Platas-Garza, J.A. de la O Serna, "Dynamic Phasor and Frequency Estimates Through Maximally Flat Differentiators," *IEEE Trans. on Instrumentation and Measurement*, vol. 59, no. 7, pp. 1803-1811, Jul. 2010.

[28] EN 50160:2010, *Voltage characteristic for electricity supplied by public distribution network*.

[29] D. Belega, D. Petri, "Accuracy Analysis of the Multicycle Synchrophasor Estimator Provided by the Interpolated DFT Algorithm," *IEEE Trans. on Instrumentation and Measurement*, vol. 62, no. 5, pp. 942-953, May 2013.

[30] D. Belega, D. Dallet, D. Petri, "Statistical Description of the Sine-Wave Frequency Estimator Provided by the Interpolated DFT Method," *Measurement*, vol. 51, no. 1, pp. 109-117, Jan. 2012.

[31] M. Bertocco, C. Narduzzi, F. Tramarin, "Characterization of Microgrid Smart Metering: Phasor Estimation under Impaired Conditions," Proc. *IEEE Int. Instrumentation and Measurement Technology Conference* (I2MTC), Minneapolis, MN, USA, pp. 1170-1175, May 2013.

[32] K. Duda, S. Barczentewicz, "Interpolated DFT for $\sin^{\alpha}(x)$ windows," *IEEE Transactions on Instrumentation and Measurement*, vol. 63, no. 4, pp. 754-760, Apr. 2014.

[33] P. Romano, M. Paolone, "Enhanced Interpolated-DFT for Synchrophasor Estimation in FPGAs: Theory, Implementation, and Validation of a PMU Prototype," *IEEE Transactions on Instrumentation and Measurement*, vol. 63, 2014.

[34] A. H. Nuttall, "Some Windows with Very Good Sidelobe Behavior," *IEEE Trans on Acoustic, Speech and Signal Processing*, vol. ASSP-29, no. 1, Feb. 1981.

[35] C. M. De Dominicis, P. Ferrari, A. Flammini, S. Rinaldi, M. Quarantelli, "On the Use of IEEE 1588 in Existing IEC 61850-Based SASs: Current Behavior and Future Challenges," *IEEE Trans. Instrumentation and Measurement*, vol. 60, no. 9, pp. 3070-3081, Sep. 2011.